UDC621.746.56:669-147:681.3:519.6

Development and Application of Simulator for Analyzing Molten Steel Flow and Inclusion Behavior in Continuous Casters

Ikuo Sawada*1
Eiichi Takeuchi*1
Hiroyuki Tanaka*3
Kensuke Okazawa*1
Kiyoshi Shigematsu*2

Abstract

Using a large eddy simulation (LES) turbulence model and the finite difference method in the three-dimensional curvilinear coordinate system, a numerical simulator was developed for analyzing the flow of molten steel in the continuous caster in the continuous casting process, the behavior of inclusions in the molten steel, and the accumulation behavior of the inclusions in the slab being cast. To verify the simulator's fluid flow computational accuracy, the results produced by the simulator were compared with the results of water and mercury model experiments. The numerical simulator was confirmed to be able to provide practically accurate predictions for not only time-averaged flow velocity, but also for turbulent fluctuation behavior. The behavior of inclusions under various continuous caster operating conditions (such as the caster profile, electromagnetic braking, and electromagnetic stirring) was analyzed by the simulator, and the main mechanisms governing the behavior of inclusions were studied.

1. Introduction

The flow of molten steel in the continuous caster in the continuous casting process is an important factor that governs the occurrence in cast steel products of internal defects, resulting from such causes as nonmetallic inclusions and argon gas bubbles, and subsurface and surface defects, stemming from such sources as mold powder, argon gas bubbles, inclusions, and longitudinal cracks due to unevenness of initial solidification. Generally, internal defects are influenced by the downward flow of molten steel after impinging on the narrow face of the mold. Surface defects are influenced by the flow of molten steel near the mold meniscus and between the submerged nozzle and the wide face of the solidifying shell. To control these molten steel flow conditions, such attempts are made as changing the geometrical shape of the submerged nozzle, electromagnetically stirring the molten steel, which involves applying a moving magnetic field to the molten steel, and applying a electromagnetic brake to the molten steel in the form of a direct-current magnetic field.

The progress of computers has increased the frequency by which numerical fluid flow computation is used to analyze the flow of molten steel in continuous casting. There are, however, few examples of such analyses being conducted with high enough quantitative accuracy. Molten steel flow and inclusion behavior models are yet to be fully studied in view of the application of direct-current and alternating-current electromagnetic fields, curved profile of the continuous caster, and shape of the solidifying shell.

*1 Technical Development Bureau
*2 Oita Works
*3 Yawata Works

This paper describes the development and application of a mathematical model and a numerical simulator that can quantitatively predict the flow of molten steel in the continuous caster and the concentration distribution of inclusions in the molten steel and the cast slab. Selection of a turbulence model is important in computing molten steel flow. The present work adopted a large-eddy simulation (LES[1]) model that has come into widespread use as a non-steady state turbulent flow computational technique in recent years. A numerical computation program, based on the finite difference method in the three-dimensional curvilinear coordinate system[2], was developed and applied to take the curved profile of the continuous caster into account. The phenomena occurring in industrial continuous casters as analyzed by using the program are described next.

2.Mathematical Model and Numerical Simulator

2.1 Basic equations

The basic equations of the mathematical model and numerical simulator are shown next. The equations of conservation of mass and momentum were used for the computation of fluid flow. Convection-diffusion balance equations that take the terminal velocity of inclusion particles into account were used for calculating the concentration of inclusions in the molten steel. The computation of the electromagnetic force (Lorentz force) used different techniques for electromagnetic braking and electromagnetic stirring.

The equation of conservation of mass, equation of conservation of momentum based on LES, and inclusion concentration balance equations follow:

$$\partial U_l/\partial t + \partial E_l/\partial \xi + \partial F_l/\partial \eta + \partial G_l/\partial \zeta = g + F \quad \cdots\cdots(1)$$

$$U_l = JU \quad \cdots\cdots(2)$$

$$E_l = J(E\xi_x + F\xi_y + G\xi_z) \quad \cdots\cdots(3)$$

$$F_l = J(E\eta_x + F\eta_y + G\eta_z) \quad \cdots\cdots(4)$$

$$G_l = J(E\zeta_x + F\zeta_y + G\zeta_z) \quad \cdots\cdots(5)$$

$$U = (\rho, \rho u, \rho v, \rho w, \rho C) \quad \cdots\cdots(6)$$

$$E = (\rho u, \rho u^2 + p + \tau_{xx}, \rho uw + \tau_{xy}, \rho uw + \tau_{xz}, \rho uC + T_x) \quad \cdots(7)$$

$$F = (\rho v, \rho uv + \tau_{xy}, \rho v^2 + p + \tau_{yy}, \rho vw + \tau_{yz}, \rho vC + T_y) \quad \cdots(8)$$

$$G = (\rho w, \rho uw + \tau_{xz}, \rho vw + \tau_{yz}, \rho w^2 + p + \tau_{zz}, p[w + w_g]C + T_z) \quad \cdots\cdots(9)$$

$$J = \partial(x,y,z)/\partial(\xi,\eta,\zeta) \quad \cdots\cdots(10)$$

t: Time
x,y,z: Cartesian coordinates
ξ,η,ζ: Curvilinear coordinates
ρ: Density
U: Flow velocity vector
τ:Sum of stress tensor based on molecular viscosity and stress tensor due to subgrid scale eddies. Simple Smagorinsky model used as subgrid scale model
p: Pressure
g: Acceleration of gravity
F: Lorentz force
w_g:Terminal flotation velocity vector of inclusion particles
T:Sum of diffusion flux based on molecular diffusion and diffusion flux due to subgrid scale eddies

Equations of electromagnetic field (for electromagnetic braking)

$$B = \mu(1/4\pi)(I\, dl \times r/r^3) \quad \cdots\cdots(11)$$

$$\mathrm{div}(\mathrm{grad}\phi) = \mathrm{div}(U \times B) \quad \cdots\cdots(12)$$

$$J = \sigma(-\mathrm{grad}\phi + U \times B) \quad \cdots\cdots(13)$$

$$F = J \times B \quad \cdots\cdots(14)$$

μ: Magnetic permeability
J: Eddy current density vector
ϕ: Electric scalar potential
B: Magnetic flux density vector

Electromagnetic field equations for electromagnetic stirring.

The basic equations based on the vector potential A-scalar potential ϕ method were used and solved by the finite element program FLEDY[3] developed by Nippon Steel.

2.2 Discretization and solution algorithms

The complete conservation-type finite difference method was used for discretization of Eqs. (1) to (13), and a staggered system was used to arrange the grid points and variables. The difference accuracy of the second to fourth terms on the left side of Eq. (1) was basically taken as second-order accuracy. Fluid flow and pressure were solved as coupled by the semi-implicit fractional step method[4] or HSMAC method[4]. The Nippon Steel-developed software FLODIA[5] was used for the above-mentioned numerical solution methods.

3. Analytical Objects

3.1 Physical model experiments for verification of computational accuracy

1) Water model experimental apparatus
Model size: 200 × 1,250 mm
Casting speed: Equivalent to 1.6 m/min
Submerged nozzle: Port size of 70 × 80 mm and port angle of 15 downward
Velocity measuring method: Time-averaged velocity measured with electromagnetic velocity meter

2) Mercury model experimental apparatus
Model size: 100 × 600 mm
Casting speed: Equivalent to 0.39 m/min
Submerged nozzle: Port size of 28 mmϕ and port angle of 15 downward
Velocity measuring method: Velocity time variation and turbulent energy spectrum measured with Vives sensor[6]

3.2 Application to industrial continuous casters

The mathematical model and numerical simulator were applied to the analysis of molten steel flow and inclusion behavior in various continuous casters at Nippon Steel. The equipment data and operating conditions of the continuous casters are omitted here.

4. Analytical Results and Discussion

4.1 Verification of fluid flow computation accuracy by water and mercury model experiments

Fluid flow computation corresponding to the water model experiment was performed by the LES method, and time averaging operation was conduced over 60 seconds. The results are shown in **Fig. 1**. The time-averaged velocity vectors obtained in the water model experiment are shown in **Fig. 2**. The calculated and measured velocities near the meniscus are comparatively shown in **Fig. 3**. From **Fig. 3**, it is evident that accurate results were achieved when the time-averaged velocity was computed by the LES method[7].

The computational results of turbulent fluctuation behavior are described next. **Fig. 4** shows the time variation of the transverse velocity component near the meniscus as calculated by the LES method. **Fig. 5** shows the time variation of the transverse

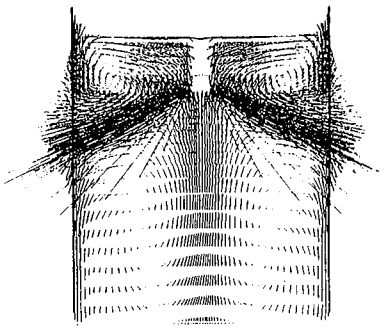

Fig. 1 Computational results of time-averaged flow velocity in water model

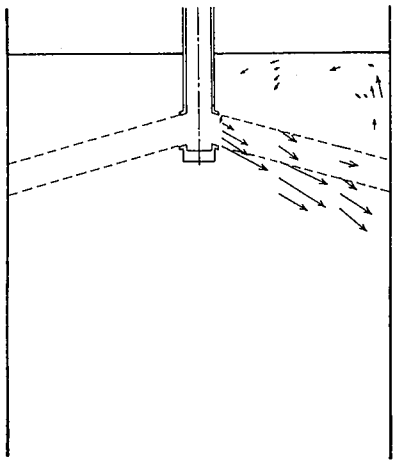

Fig. 2 Experimental results of time-averaged flow velocity in water model

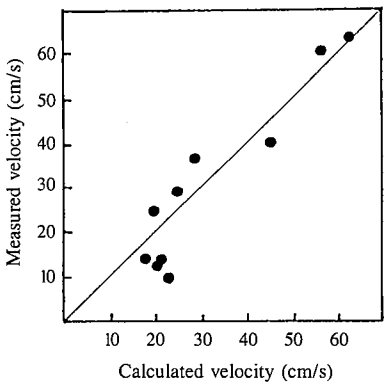

Fig. 3 Comparison of calculated and measured time-averaged flow velocities in water model

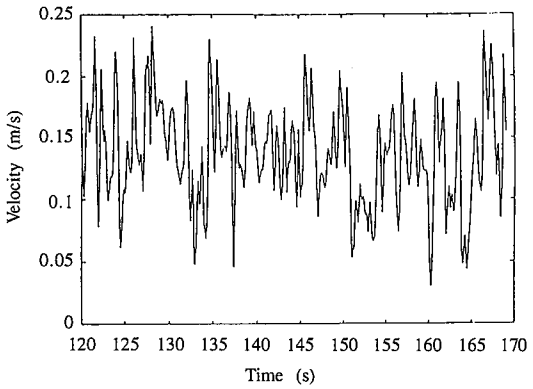

Fig. 4 Change with time in flow velocity near meniscus as calculated by LES method

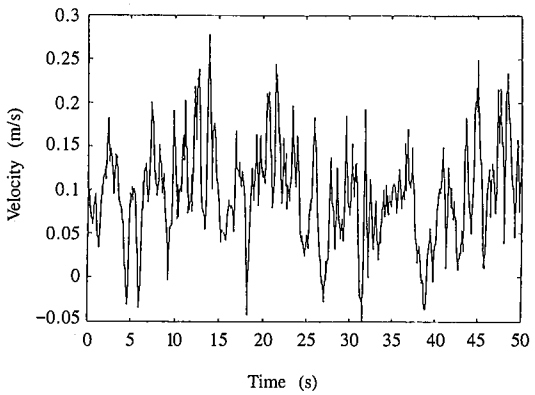

Fig. 5 Change with time in flow velocity near meniscus as measured in mercury model

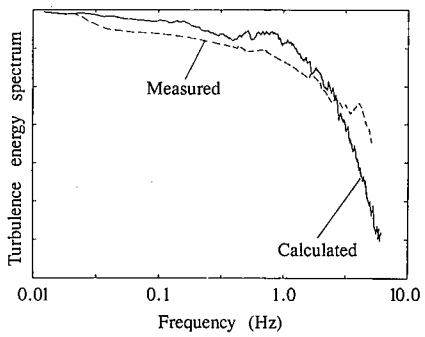

Fig. 6 Comparison of calculated and measured turbulence energy spectra near meniscus

velocity component near the meniscus as measured by the mercury model experiment. Variations of a similar nature are observed between the calculated results and the measured results. **Fig. 6** shows the comparison of the turbulence energy spectrum velocity near the meniscus as calculated by the LES method and as measured by the mercury model experiment. Obtained were qualitatively common results such as strong turbulent components are present in a wide frequency region of 0.01 Hz to a few Hertz, and turbulence energy suddenly decays at a frequency of a few Hertz or more.

As a result of the study using the turbulent fluctuation analytical technique, it was discovered that the formation of turbulent flow present in the upper part of the continuous caster mainly originates from the instability of flow near the ports of the submerged nozzle.

4.2 Numerical analysis of molten steel flow and inclusion accumulation behavior by consideration of machine profile

Using three-dimensional generalized coordinate conversion, molten steel flow and inclusion behavior were analyzed to take into account the effects of the curved machine profile, such as the bow type or vertical bending type, and the solidifying shell shape.

The slab size was 289 × 1,830 mm, the casting speed was 1.3 m/min, and the machine profile was either the vertical-bending type (vertical section of 2.5 m) or bow type (radius of 10.5 m).

Fig. 7 shows the computational results of molten steel flow in continuous casters of the vertical-bending type and the bow type. With the bow type, the curved flow path resists and reduces the downward flow of the molten steel. In terms of the accumulation of inclusions in the cast slab, this result appears to favor the bow type but the bow type actually has an adverse effect on the accumulation of inclusions in the slab as described below.

Fig. 8 shows the calculated through-thickness distributions of 280-μm inclusions in the slabs cast on machines of the vertical bending type and bow type. **Fig. 9** shows the measured through-thickness distributions of 280-μm particles in the slabs cast under the operating conditions with approximately the same flotation parameter (equal to terminal inclusion flotation velocity divided by casting speed) as shown in **Fig. 8**. Generally speaking, the calculated values agree with the measured values.

With the bow type, a strong inclusion accumulation phenomenon can be seen approximately 30 mm below the loose-side surface of the slab. This peak position corresponds to the solidification position where the curve of the machine beings to increase. The peak value is greater than observed with the vertical-bending type. This finding indicates that the curved profile of the machine has a greater effect than the flow of the molten steel on the accumulation phenomenon of inclusions in the cast slab. In other words, the trap velocity of inclusions into the solidifying shell in positions deep below the meniscus depends on the inner product of the terminal flotation velocity vector of inclusions (in the direction opposite to gravity), and the normal vector at the solid-liquid interface. As the solid-liquid interface comes closer to the horizontal condition, the inclusions are more liable to be trapped in the solidifying shell. Actually, the amount of inclusions trapped in the 2.5-m vertical section of the vertical-bending machine was extremely small.

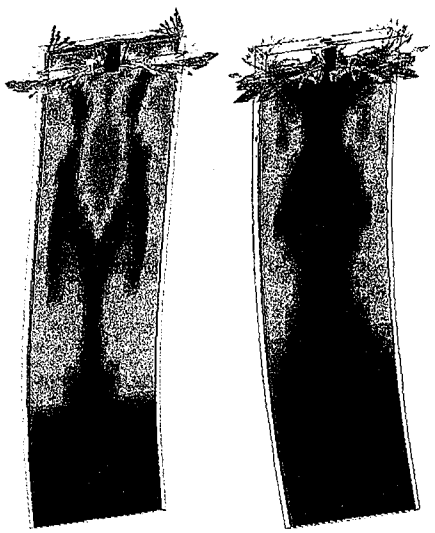

(a) Vertical-bending type (b) Bow type

Fig. 7 Computational results of molten steel flow velocity in continuous caster (half section in thickness direction)

4.3 Effect of electromagnetic braking in continuous slab caster

If the casting conditions are the same as discussed previously, the curved profile of the machine has the most pronounced effect on the internal accumulation behavior of inclusions in the slab. If the machine profile is the same, the same effect of molten steel flow appears. The inclusions do not sink deep into the mold, particularly when the downward velocity of the circulating molten steel flow formed in the lower part of the mold is lower than their terminal flotation velocity. When the downward velocity of the molten steel flow is higher than their terminal flotation velocity, the inclusions sink deep into the mold and are trapped more in the internal accumulation zone. Of late, a direct-current magnetic field electromagnetic brake has been applied as one method for controlling the downward flow of molten steel.

Fig. 10 shows the calculated flow of the molten steel to which an electromagnetic brake was applied, forming a uniform horizontal magnetic field at a depth of 1.1 m below the meniscus. Compared with the calculated flow of non-electromagnetically-braked molten steel as shown in **Fig. 11**, it is evident that the downward velocity of the molten steel is reduced immediately below the magnetic field and that the molten steel stops circulating.

4.4 Effect of electromagnetic stirring in continuous slab caster

Because the trapping position is near the meniscus and the

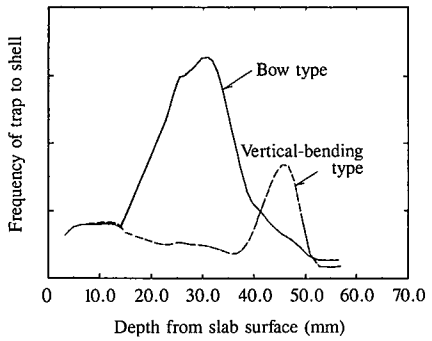

Fig. 8 Calculated through-thickness distribution of inclusions in slab

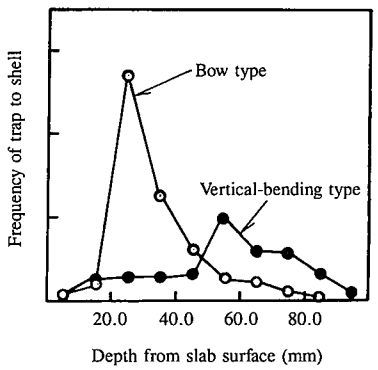

Fig. 9 Through-thickness distribution of inclusions observed in slab

liquid-solid interface is nearly vertical, and due to the floating of inclusions as decribed earlier, the trapping behavior of inclusions in the subsurface of the slab is not governed by their trapping phenomenon. Sawada et al. reported that increasing molten steel flow velocity reduces the captures of inclusions in the slab and diminishes the size of inclusions trapped (see **Fig. 12**)[8]. This phenomenon is interpreted as the washing out of the inclusions by the molten steel. To promote this shell washing phenomenon, the molten steel is electromagnetically stirred with a moving magnetic field to increase flow velocity.

The computational results of molten steel poured from a round submerged nozzle with and without electromagnetic stirring are shown in **Figs. 13** and **14**, respectively. The effect of electromagnetic stirring is more conspicuous near the center of the liquid core than near the meniscus. Compared with the non-electromagnetically-stirred molten steel, the electromagnetically-stirred molten steel increases in flow velocity near the solid-liquid interface. When considered together with the results of Sawada et al. this finding agrees with the fact that electromagnetic stirring sharply reduces the number of large inclusions.

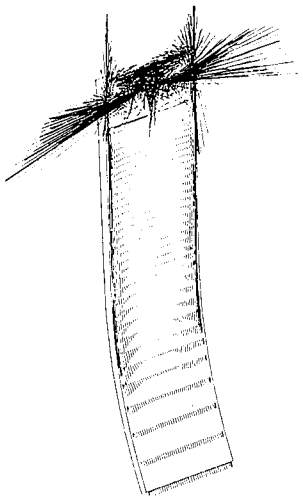

Fig. 10 Computational results of molten steel flow with electromagnetic braking

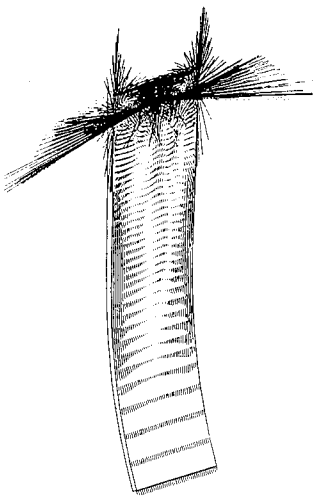

Fig. 11 Computational results of molten steel flow without electromagnetic braking

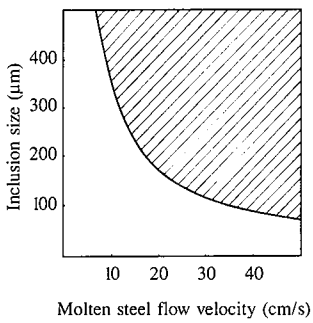

Fig. 12 Effects of molten steel flow velocity and inclusion size on inclusion shell washing (shell washing region is hatched)

5. Conclusions

Using the LES turbulence model and the finite difference method in the three-dimensional curvilinear coordinate system, a numerical simulator was developed for calculating the flow of molten steel in the continuous caster, the behavior of inclusions

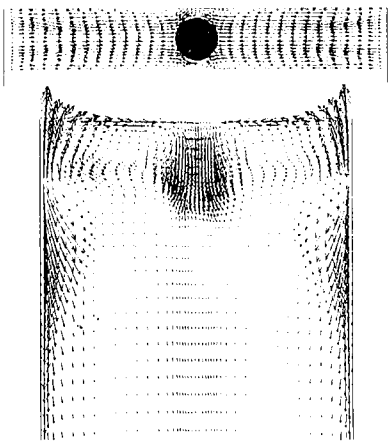

Fig. 13 Computational results of molten steel flow without electromagnetic stirring

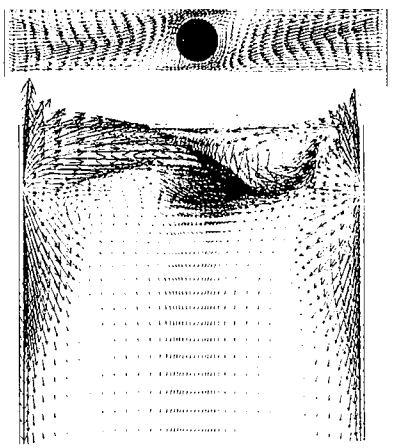

Fig. 14 Computational results of molten steel flow with electromagnetic stirring

in the molten steel, and the accumulation behavior of the inclusions in the slab being cast in the continuous caster.

To verify the computational accuracy of the simulator, the results of calculations by the simulator were compared with the results of water and mercury model experiments. The simulator was confirmed to be practically accurate for not only time-averaged flow velocity, but also for turbulent fluctuation behavior. The trapping behavior of inclusions in the slab was analyzed under various continuous caster operating conditions by using the numerical simulator. The results obtained helped to understand the mechanisms that govern the trapping behavior of inclusions in the slab being cast in the continuous caster.

References

1) Deadorff, J.W.: Fluid Mecha. 41, (1970)
2) Anderson, D.A., Tannehill, J.C., Pletcher, R.H.: Computational Fluid Dynamics and Heat Transfer. McGraw-Hill,1984
3) Ueyama, T., Shinkura, K., Ueda, R.: IEEE Trans. Magn. 25, 4113k (1989)
4) Tanahashi, T.: Kikai no Kenkyu. 39, 1249 (1987)
5) Sawada, I., Tanaka, H., Tanaka, M.: BRS Bulletin. 14 (1994)
6) Vives, C.H., Ricou, R.: Met. Tans. 168, 377 (1985)
7) Sawada, I., Kishida, Y., Okazawa, K., Tanaka, H.: Tetsu-to-Hagané. 79, 30 (1993)
8) Sawada, I., Okazawa, K.: CAMP-ISIJ. 8 (1), 344 (1995)